

Osteoclast-derived IGF1 is required for pagetic lesion formation in vivo

Kazuaki Miyagawa,¹ Yasuhisa Ohata,¹ Jesus Delgado-Calle,¹ Jumpei Teramachi,¹ Hua Zhou,² David D. Dempster,³ Mark A. Subler,⁴ Jolene J. Windle,⁴ John M. Chirgwin,¹ G. David Roodman,^{1,5} and Noriyoshi Kurihara¹

¹Division of Hematology and Oncology, Department of Medicine, Indiana University (IU), Indianapolis, Indiana, USA.

²Regional Bone Center, Helen Hayes Hospital, West Haverstraw, New York, USA. ³Department of Clinical Pathology and Cell Biology, Columbia University, New York, New York, USA. ⁴Department of Human and Molecular Genetics, Virginia Commonwealth University (VCU), Richmond, Virginia, USA. ⁵Roudebush VA Medical Center, Indianapolis, Indiana, USA.

We report that transgenic mice expressing measles virus nucleocapsid protein (MVNP) in osteoclasts (OCLs) (*MVNP* mice) are Paget's disease (PD) models and that OCLs from patients with PD and *MVNP* mice express high levels of OCL-derived IGF1 (OCL-IGF1). To determine OCL-IGF1's role in PD and normal bone remodeling, we generated WT and *MVNP* mice with targeted deletion of *Igf1* in OCLs (*Igf1*-cKO) and *MVNP/Igf1*-cKO mice, and we assessed OCL-IGF1's effects on bone mass, bone formation rate, EphB2/EphB4 expression on OCLs and osteoblasts (OBs), and pagetic bone lesions (PDLs). A total of 40% of *MVNP* mice, but no *MVNP/Igf1*-cKO mice, had PDLs. Bone volume/tissue volume (BV/TV) was decreased by 60% in lumbar vertebrae and femurs of *MVNP/Igf1*-cKO versus *MVNP* mice with PDLs and by 45% versus all *MVNP* mice tested. Bone formation rates were decreased 50% in *Igf1*-cKO and *MVNP/Igf1*-cKO mice versus WT and *MVNP* mice. *MVNP* mice had increased EphB2 and EphB4 levels in OCLs/OBs versus WT and *MVNP/Igf1*-cKO, with none detectable in OCLs/OBs of *Igf1*-cKO mice. Mechanistically, IL-6 induced the increased OCL-IGF1 in *MVNP* mice. These results suggest that high OCL-IGF1 levels increase bone formation and PDLs in PD by enhancing EphB2/EphB4 expression in vivo and suggest OCL-IGF1 may contribute to normal bone remodeling.

Introduction

Paget's disease (PD) is the most exaggerated example of coupled bone remodeling, with highly localized areas of increased bone resorption, accompanied by exuberant new bone formation (1). The rapid, excessive, focal deposition of new bone in PD results in woven bone that is much weaker, can bow and cause bone deformity, can fracture, exhibits skull thickening, causes bone pain, shows signs of secondary osteoarthritis, and shows signs of nerve root compression (2). The primary cellular abnormality in PD resides in the osteoclast (OCL) (3). OCLs in PD (PD-OCLs) are increased in number and size, are hypermultinucleated, and have increased 1,25-(OH)₂D₃ and RANKL responsiveness compared with normal OCLs (4–7). Furthermore, PD-OCLs secrete high levels of IL-6, which are detectable in the marrow and peripheral blood of patients with PD (8). OCLs drive the increased bone formation in PD because treatment with bisphosphonates, which decreases OCL activity, blocks new pagetic bone formation (2). These findings suggest that PD offers key insights into processes that link bone resorption and formation.

We previously reported that OCLs from 70% of patients with PD express the measles virus nucleocapsid protein (*MVNP*) gene, and transgenic mice with *MVNP* targeted to OCLs (*MVNP* mice) develop OCLs and bone lesions characteristic of PD (9). Importantly, *MVNP* mice lacking IL-6 expression do not develop pagetic-like OCLs and increased new bone formation in vivo (9). However, the mechanisms responsible for the increased bone formation in PD have not been clearly elucidated in vivo.

Normal bone resorption and formation are tightly linked, with bone formation occurring only at sites of previous bone resorption. This coupling of bone remodeling results from communication between OCLs and osteoblasts (OBs) (10). Several studies implicated expression of Eph receptors on OBs and ephrins on OCLs and OBs as major regulators of coupling (11, 12). We recently reported that *MVNP*-expressing OCLs from patients with PD and *MVNP* mice express high levels of IL-6, IGF1, and EphB2 (13).

Authorship note: KM and YO contributed equally to this work

Conflict of interest: The authors have declared that no conflict of interest exists.

Copyright: © 2020, American Society for Clinical Investigation.

Submitted: September 3, 2019

Accepted: February 19, 2020

Published: March 26, 2020.

Reference information: *JCI Insight*. 2020;5(6):e133113.
<https://doi.org/10.1172/jci.insight.133113>.

The high levels of OCL-derived IL-6 induced IGF1 and EphB2 in OCLs, and EphB4 on OBs, to increase OB differentiation in vitro (13). Furthermore, we previously reported that EphB4-Fc treatment of OCL precursors from WT and *MVNP* mice inhibited OCL formation, decreased bone resorption, and abrogated the effects of MVNP on the expression of a pagetic phenotype by the OCLs that formed. In addition, EphB2-Fc treatment inhibited OB differentiation, decreased Rho signaling in both WT and *MVNP* OB precursors, and blocked the increased OB differentiation induced by coculture with *MVNP*-expressing OCLs (*MVNP*-OCLs) (13). We found that OCLs, rather than OBs, are the major producer of local IGF1 in PD and that the amount of IGF1 produced by *MVNP*-expressing OCLs is considerable. Several studies reported a role for IGF1 in coupling bone resorption and formation, but they focused on the effects of bone matrix-derived IGF1, released by osteoclastic bone resorption, on OB differentiation and new bone formation (14, 15). These reports showed that IGF1 signaling in OBs enhanced the expression and secretion of RANKL (16) and that new bone formation induced by IGF1 occurred at bone resorption sites to maintain normal bone remodeling (14). However, the role of OCL-derived IGF1 (OCL-IGF1) in PD and physiologic bone remodeling in vivo is unknown.

In this study, we examined the mechanisms responsible for the effects of OCL-IGF1 on the increased bone formation and development of pagetic bone lesions (PDLs) in PD and on physiologic bone remodeling in vivo. We generated potentially novel mouse models with conditional deletion of *Igf1* in OCLs of WT and *MVNP* mice by breeding *Tracp-Cre* or *MVNP/Tracp-Cre* with *Igf1^{fl/fl}* mice. PDLs were detected in 18- to 24-month-old *MVNP* mice but not in the other genotypes. Notably, bone volume/tissue volume (BV/TV) of *MVNP/Igf1*- conditional KO (*VNP/Igf1-cKO*) vertebrae and femurs was decreased by 60 % versus *MVNP* mice with PDL and by 45% versus BV/TV in all *MVNP* mice tested. Furthermore, bone formation rates (BFRs) in *Igf1-cKO* and *MVNP/Igf1-cKO* mice were decreased 50% compared with WT and *MVNP* mice, respectively. Additionally, expression of EphB2 and EphB4 in *MVNP/Igf1-cKO* mice was very low compared with *MVNP* mice and was undetectable in *Igf1-cKO* mice in vivo. Finally, we showed that OCLs in bone sections from a PD patient expressed high levels of IGF1. Thus, our results suggest OCL-IGF1 (a) increases bone formation, (b) is required for development of PDL in PD through increased EphB2/EphB4 expression in OCLs and OBs, and (c) possibly contributes to adult physiological bone remodeling in vivo.

Results

IGF1 expression in OCLs and BFRs are increased in bone samples from a patient with PD. To determine if IGF1 expression was increased in OCLs of patients with PD in vivo, we performed histologic analysis of bone samples from a PD patient and a healthy donor. The OCLs in the PD bone sample were large, hypermultinucleated, and resided in deep resorption cavities characteristic of PD (Figure 1A). In contrast, OCLs in the normal bone specimen were smaller, had fewer nuclei/OCL, and resided in shallower resorption pits. In addition, immunostaining of the bone sections with anti-IGF1 antibody showed that OCLs from the PD patient had much stronger staining compared with OCLs in normal bone (Figure 1B). Furthermore, dynamic histomorphometric analyses of these calcein-labeled bone specimens showed that the mineral apposition rate (MAR) and BFR were higher in the PD patient than the healthy donor sample (Figure 1C), suggesting a potential link between high OCL-IGF1 and increased bone formation in PD.

Specificity of TRACP-Cre expression in OCL lineage cells in bone. To characterize the role of increased OCL-IGF1 in the increased bone formation in PD, we bred *TRACP-Cre* transgenic mice to *Igf1*-floxed mice to delete *Igf1* in the OCL lineage. However, we first confirmed the specificity of the *TRACP* promoter to OCLs in bone by breeding *TRACP-Cre* mice to the Ai9 reporter mouse strain that contains a CAG promoter, followed by a *loxP*-flanked STOP cassette and the coding region of a red fluorescent protein variant (tdTomato) (17). In cells expressing Cre, the STOP cassette is deleted, resulting in strong Tomato red fluorescence. The localization of *TRACP*⁺ OCLs and anti-Tomato immunopositive OCLs is shown in Supplemental Figure 1 (supplemental material available online with this article; <https://doi.org/10.1172/jci.insight.133113DS1>). Using sequential sections, we found that *TRACP* and Tomato staining colocalized in OCLs from *Tracp-Cre(+)/Tomato* mice, as shown by the arrows, whereas OCLs in *Tracp-Cre(-)/Tomato* bones were not stained by the anti-Tomato antibody. The anti-Tomato antibody also weakly stained occasional osteocytes (OCys) in bone.

Since targeted disruption of the *Igf1* gene in OCys impairs developmental bone growth in mice, we examined if OCy IGF1 expression was affected in OCys in *Igf1-cKO* mice. Immunostaining of OCys with an anti-IGF1 antibody showed similar levels of IGF1 staining of OCys from 4 genotypes (Supplemental Figure 2). Furthermore, Western blotting of lysates and ELISA assays of OCy conditioned media

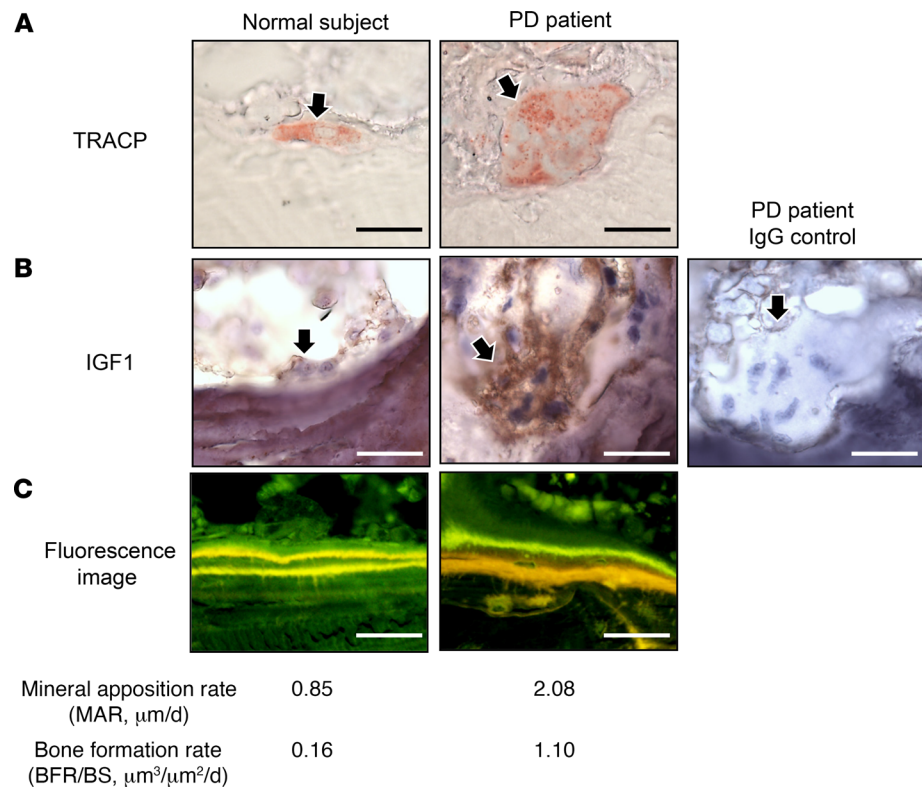


Figure 1. OCL phenotype and remodeling in Paget's patient and healthy donor bone. (A) OCLs were stained with TRACP. (B) Detection of IGF1. IGF1 expression was determined by immunostaining using anti-IGF1 antibody as described in Methods. TRACP and IGF1 staining were performed on consecutive sections. (C) New bone formation. Mineral apposition rates and new bone formation rates were measured as described in Methods. Scale bars: 100 μm . All data shown are typical of 3 technical replicates. The information on the PD patient and healthy donor is described in Methods. Arrows denote an osteoclast.

of WT, *Igf1*-cKO, *MVNP*, and *MVNP/Igf1*-cKO showed that IGF1 expression levels were similar for all 4 genotypes (Supplemental Figure 2). The amounts of IGF1 secreted by OCys from the 4 genotypes were much lower than these secreted by *MVNP*-OCLs (20 pg/mL/ 2×10^5 OCys versus 200 pg/mL/ 5×10^4 OCLs). Based on these data, we concluded that cKO of *Igf1* using *TRACP-Cre* did not significantly affect IGF1 expression by OCys.

Effects of Igf1 deletion in OCLs on the size, weight, femoral length, IGF1, and IGFBP3 levels in 4 genotype mice. To examine the effects of *Igf1* deletion in OCLs of WT and *MVNP* mice, we generated cohorts of mice of the following 4 genotypes: (a) *Igf1*^{fl/fl} (WT), (b) *TRACP-Cre*(+)/*Igf1*^{fl/fl} (*Igf1*-cKO), (c) *TRACP-MVNP/Igf1*^{fl/fl} (*MVNP*), and (d) *TRACP-MVNP/TRACP-Cre/Igf1*^{fl/fl} (*MVNP/Igf1*-cKO). Lack of OCL-*Igf1* had no effect on the size, weight, and femur length of WT or *MVNP* mice at 12–24 months of age. In addition, serum IGF1 and IGFBP3 levels were unchanged by the absence of OCL-*Igf1* (Supplemental Figure 3). TRACP expression levels in liver, which is the major source of IGF1 and can express TRACP, were almost undetectable compared with OCLs, as assessed by Western blot (data not shown). Interestingly, mice with targeted deletion of *Igf1* in OCLs, either with or without *MVNP*, were born at much-lower-than-expected numbers (~25% instead of the expected 50%). Since TRACP is expressed in the kidney, we also analyzed if 1,25-(OH)₂D₃ produced by kidney is affected in the *Igf1*-cKO mice. The serum levels of 1,25-(OH)₂D₃ in WT mice (38.2 ± 5.2 pg/mL, *n* = 5), *Igf1*-cKO mice (39.3 ± 5.8 pg/mL, *n* = 5), *MVNP* mice (43.4 ± 3.3 pg/mL, *n* = 5), and *MVNP/Igf1*-cKO mice (45.6 ± 7.3 pg/mL, *n* = 5) were not significantly different.

Genetic deletion of Igf1 in OCLs prevents PDL formation in MVNP mice. WT, *Igf1*-cKO, *MVNP*, and *MVNP/Igf1*-cKO mice (18–24 months of age) were examined for the presence of PDLs. Mice of this age were examined because we most consistently find PDLs in *MVNP* mice at 12 months of age or older (9). PDLs were detectable in 40% of *MVNP* mice (4 of 10) by μCT (Table 1) and histological analysis, and they were found in vertebrae, femurs, and tibiae at 18–24 months of age (Supplemental Figure 4 and Supplemental

Table 1. The number of mice and PDLs in transgenic or WT mice

	WT	Igf1-cKO	MVNP	MVNP/Igf1-cKO
Number of mice	8	8	10	6
Pagetic Lesions	0	0	4	0

PDLs were screened by μ CT as described in Methods. Markedly abnormal bone structure was seen 4 of the 10 MVNP mice (40%) at 18–24 months of age.

Table 1). In contrast, no PDLs were detected in any of the *MVNP/Igf1-cKO*, *Igf1-cKO*, or WT mice examined at the same age as the *MVNP* mice.

Characterization of the skeletal consequences of conditional deletion of Igf1 in WT and MVNP mice. We next determined bone volume (BV) and trabecular bone parameters in vertebrae and femurs from mice of the 4 genotypes at 20 months of age. μ CT images of vertebrae and femurs of *MVNP* mice with PDLs showed increased bone mass compared with the other genotypes (Figure 2A and Supplemental Figure 5B). BV/TV in PDLs of vertebrae from *MVNP* mice was increased 1.5-fold compared with vertebrae of *MVNP* mice without PDLs and 2.5-fold compared with WT mice ($P < 0.01$). BV/TV of vertebrae from *MVNP/Igf1-cKO* mice was decreased by 60% compared with vertebrae with PDL from *MVNP* mice and was decreased by 45% compared with BV/TV in vertebrae of all *MVNP* mice tested (Figure 2B). Notably, BV/TV in *Igf1-cKO* mice was also decreased compared with WT mice and lower than *MVNP/Igf1-cKO* mice. Trabecular number (Tb.N) in vertebrae with PDL from *MVNP* mice was significantly increased compared with vertebrae from WT mice and *MVNP* mice without PDLs ($P < 0.01$) (Figure 2B). *MVNP/Igf1-cKO* and *Igf1-cKO* mice had similar Tb.N, which was lower than Tb.N in vertebrae with PDLs from *MVNP* mice ($P < 0.01$). Conditional deletion of OCL-IGF1 decreased trabecular width (Tb.Wi) and increased trabecular separation (Tb.Sp) in vertebrae of both WT and *MVNP* mice ($P < 0.05$) and was significantly different in *MVNP* mice with/without PDLs compared with the other genotypes (Figure 2B). Similar effects on bone parameters in femurs were also found (Supplemental Figure 5A).

We then examined if OCL-IGF1 affected cortical bone structure and volume in the same mice used for trabecular bone analyses. We measured cortical bone structures in the midshaft of the tibia from the mice according to guidelines for assessment of bone microstructure in rodents using μ CT (18). No differences were detected among the 4 genotypes at 20 months of age (Figure 2C). Similarly, cortical area fraction, average cortical thickness, periosteal perimeter, and endocortical perimeter were not significantly different among the 4 genotypes (Figure 2D). We determined if our μ CT results shown in Figure 2 significantly differed in male versus female mice. The μ CT results for male versus female WT mice, *MVNP* mice without PDL, and *MVNP/Igf1-cKO* mice did not differ significantly, but results of male versus female *MVNP* mice with PDLs and *MVNP/Igf1-cKO* could not be analyzed because we only had 1 male *MVNP* mouse with a PDL and 2 male *Igf1-cKO* mice.

Histomorphometric analysis and BFRs in WT and MVNP mice with conditional deletion of Igf1 in OCLs. TRACP staining of OCLs in *MVNP* mice showed that the OCLs were larger in size and hypermultinucleated compared with WT mice analogous to PD-OCLs. As expected, the resorption cavities in *MVNP* mice appeared deeper than in the other genotypes. OCLs present in bones from WT, *Igf1-cKO*, and *MVNP/Igf1-cKO* mice displayed normal morphology and were smaller than OCLs found in *MVNP* mice (Figure 3A). Histomorphometric analyses of vertebrae for mice of the 4 genotypes at 20 months of age are shown in Figure 3, B and D. OCL surface (osteoclast surface/bone surface [Oc.S/BS]) and number (number of osteoclasts/bone perimeter [N.Oc/B.Pm]) and OB surface (osteoblast surface/bone surface [Ob.S/BS]) and number (number of osteoblasts/bone perimeter. [N.Ob/B.Pm]) were significantly increased in *MVNP* mice compared with the other genotypes. Deletion of *Igf1* in OCLs significantly decreased these parameters in both WT and *MVNP* mice. We then determined the ratio of Oc.S/BS and Ob.S/BS in vertebrae with PDLs from *MVNP* mice and in vertebrae of *MVNP* mice without PDLs (Figure 3B). In vertebrae with PDLs from *MVNP* mice, Oc.S/BS was increased 1.44-fold, N.Oc/B.Pm was increased 1.34-fold, Ob.S/BS was increased 1.48-fold, and N.Ob/B.Pm was increased 1.52-fold, compared with vertebrae from *MVNP* mice without PDLs. Histomorphometric analyses of femurs also showed that femoral PDLs in *MVNP* mice had higher bone mass compared femurs of *MVNP* mice without PDLs and mice of the other genotypes (Supplemental Figure 5C). These results show that increased numbers of OCLs and OBs are present in PDLs of *MVNP* mice compared with bones from *MVNP* mice without PDLs.

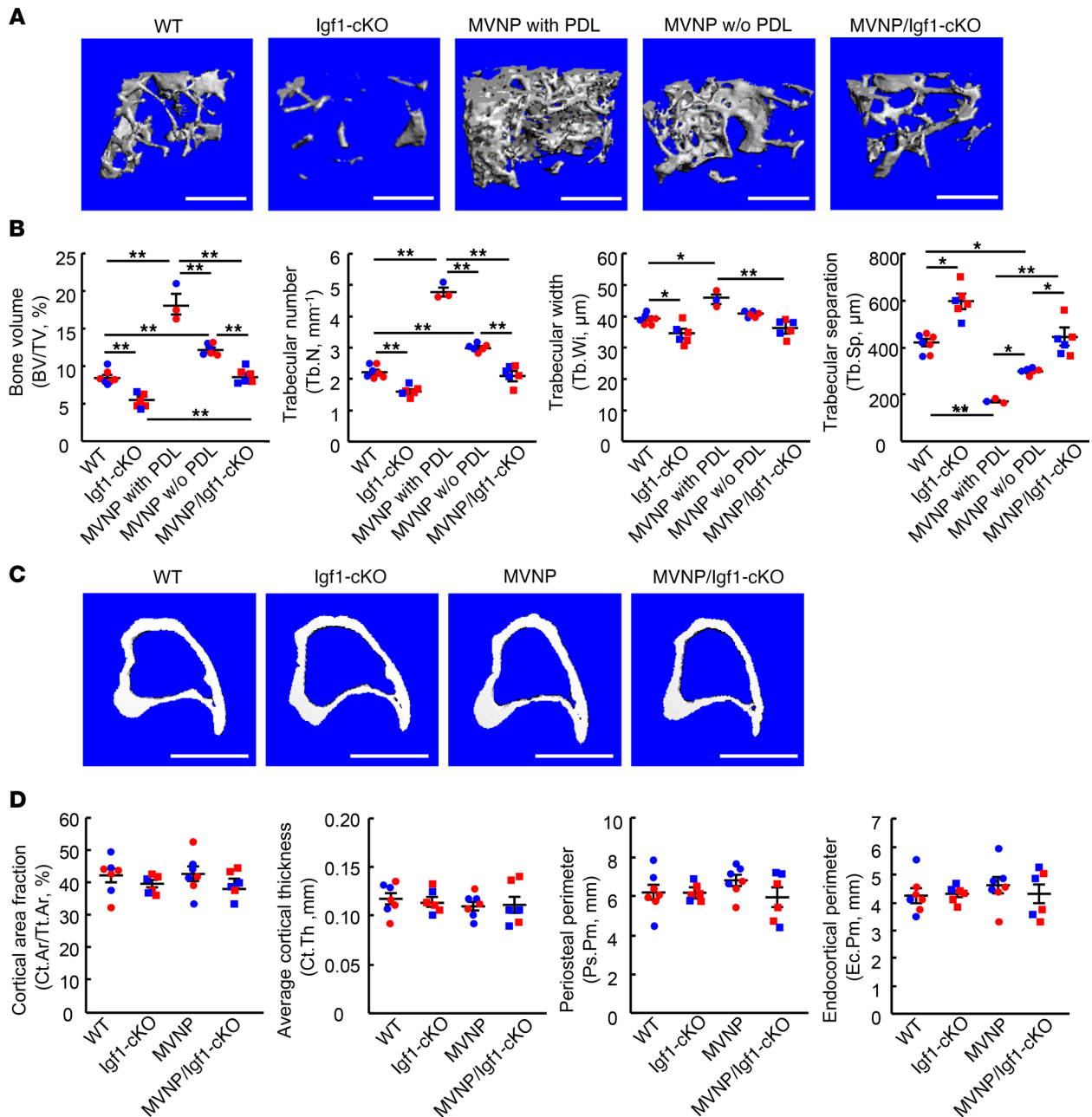


Figure 2. Bone structure and remodeling in WT, *Igf1-cKO*, *MVNP*, and *MVNP/Igf1-cKO* mice. (A) Representative μ CT images of fifth lumbar vertebra. Scale bar: 1 mm. (B) Bone volume and structural parameters of trabecular bone in vertebrae. Results are expressed as the mean \pm SEM for WT (3 male, 4 female, 19 \pm 2 months), *Igf1-cKO* (2 male, 4 female, 16 \pm 2 months), *MVNP* with PDLs (1 male, 2 female, 21 \pm 2 months), *MVNP* without PDL (3 male, 3 female, 20 \pm 1 months), and *MVNP/Igf1-cKO* (3 male, 3 female, 22 \pm 2 months old). The data were analyzed using a 1-way ANOVA with Tukey test. * $P < 0.05$. ** $P < 0.01$ as compared with each indicated group. The blue circles represent results from male mice; red circles represent results from female mice. (C) Representative μ CT images of tibia (vertical section). Scale bar: 1 mm. (D) Cortical bone parameters. Results are shown the mean \pm SEM for WT (3 male, 4 female, 19 \pm 2 months), *Igf1-cKO* (2 male, 4 female, 16 \pm 2 months), *MVNP* (4 male, 5 female, 21 \pm 2 months), and *MVNP/Igf1-cKO* (3 male, 3 female, 22 \pm 2 months) mice. The blue circles represent results from male mice; red circles represent results from female mice. Results in D were not significantly different. Results in B and D are representative of 6–9 biological replicates. Mice of similar age were used in each experiment. The μ CT results of male versus female in WT, *MVNP* without PDLs, and *MVNP/Igf1-cKO* were not statistically different. Results of male versus female *MVNP* mice with PDLs and *MVNP/Igf1-cKO* could not be analyzed because the 1 male *MVNP* mouse with PDL and 2 male *Igf1-cKO* mice were insufficient for comparison.

We next examined BFRs in calcein-labeled bones from mice of the 4 genotypes at 20 months of age. Fluorescence images of vertebral bone from these mice are shown in Figure 3C. The width of newly formed bone was markedly increased in *MVNP* mice compared with the other genotypes. Mineralizing surface (MS/BS) and MAR in *MVNP* mice were also significantly higher than in mice with cKO of OCL-

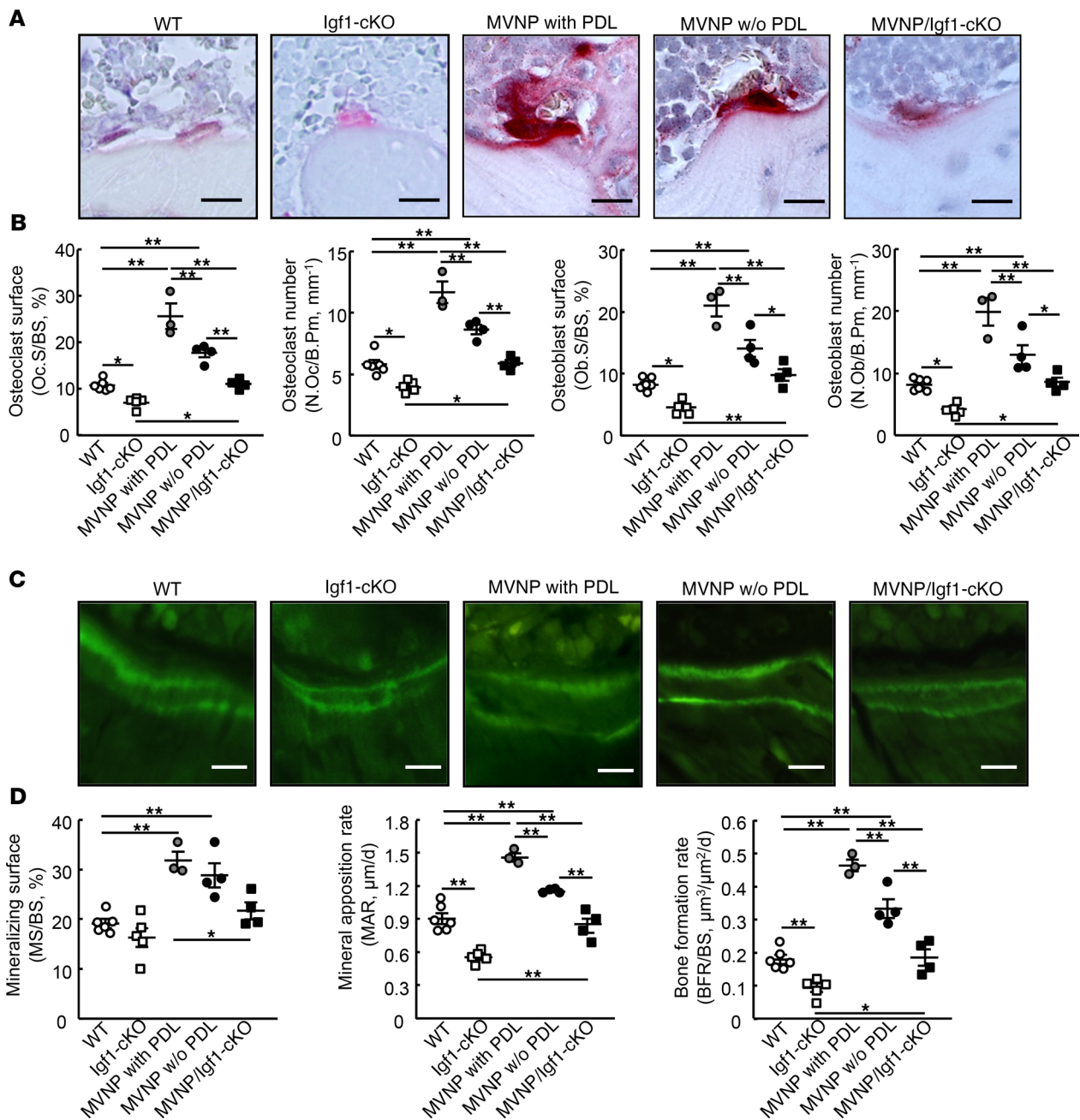


Figure 3. Histomorphometric analysis and bone formation rates in WT, *Igf1-cKO*, *MVNP*, and *MVNP/Igf1-cKO* mice. (A) OCL morphology. OCLs in vertebra sections were stained with TRACP. Scale bars: 100 μm . **(B)** Bone morphometric analysis. Results are expressed as the mean \pm SEM for WT (2 male, 4 female, 19 \pm 2 months), *Igf1-cKO* (1 male, 4 female, 16 \pm 3 months), *MVNP* with PDLs (1 male, 2 female, 21 \pm 2 months), *MVNP* without PDL (3 male, 1 female, 21 \pm 2 months), and *MVNP/Igf1-cKO* (3 male, 1 female, 25 \pm 2 months). The data were analyzed using 1-way ANOVA with Tukey test. * P < 0.05 as compared with each indicated group. **(C)** Photomicrograph of new bone formation in vertebra (L5). Scale bars: 50 μm . **(D)** Mineralized perimeter, mineral apposition, and new bone formation rates. Data are expressed as the mean \pm SEM WT (2 male, 4 female, 19 \pm 2 months), *Igf1-cKO* (1 male, 4 female, 16 \pm 3 months), *MVNP* with PDLs (1 male, 2 female, 21 \pm 2 months), *MVNP* without PDLs (3 male, 1 female, 21 \pm 2 months old), and *MVNP/Igf1-cKO* (3 male, 1 female, 25 \pm 2 months). The data were analyzed using 1-way ANOVA with Tukey test. * P < 0.05, ** P < 0.01 as compared with each indicated group. Results in **B** and **D** are representative of 4–6 biological replicates. Mice of similar age were used in each experiment.

Igf1 or WT controls (P < 0.01) (Figure 3D). Furthermore, MAR and BFR/BS in PDLs of *MVNP* mice were greater than in *MVNP* mice without PDLs (P < 0.01). Importantly, conditional deletion of *Igf1* in OCL restored these parameters to control levels in *MVNP* mice and decreased them in WT mice. These results suggest that OCL-IGF1 contributes to new bone formation in both *MVNP* and control mice.

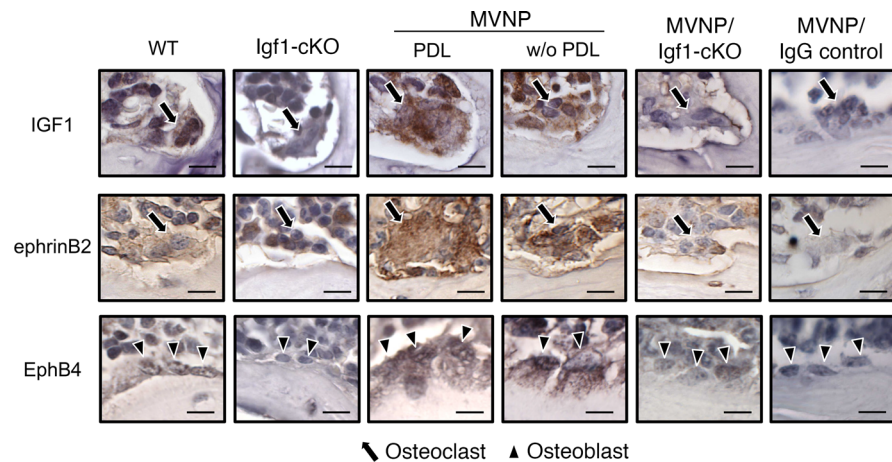


Figure 4. Detection of IGF1, EphB2, and EphB4 in bone sections of WT, *Igf1*-cKO, MVNP, and MVNP/*Igf1*-cKO mice. Femur sections from the 4 genotype mice were stained with anti-IGF1, anti-EphB2, and anti-EphB4 antibodies as described in Methods. OCLs from MVNP mice were clearly stained for IGF1 and EphB2 compared with OCLs from the other genotype mice, which showed minimal or negative staining. OBs from MVNP mice strongly stained positively for EphB4 compared with OBs from the other genotype mice. Determination of staining intensity (positive or negative) was performed by blinded observers. Arrows point to OCLs, and arrowheads point to OBs. Bones of MVNP mice stained with control IgG. Scale bars: 50 μ m. Results are representative of WT (17 months), *Igf1*-cKO (21 months), MVNP-PDL (24 months), MVNP-No PDL (21 months), and MVNP/*Igf1*-cKO (23 months old mice). Results are representative of 3 biological replicates. Mice of similar age were used in each experiment.

IGF1 deletion in OCLs decreases EphB2 and EphB4 expression of OCLs and OBs in WT and MVNP mice. To determine the mechanisms responsible for the effects of OCL-IGF1 on bone formation, femurs from 20-month-old mice were immunostained with anti-IGF1, anti-EphB2, and anti-EphB4 antibodies. As shown in Figure 4, OCLs from MVNP mice with/without PDLs expressed more IGF1 and EphB2 than OCLs from WT mice, which showed low levels of IGF1 and EphB2 expression. IGF1⁺ and EphB2⁺ OCLs were not detected in *Igf1*-cKO and MVNP/*Igf1*-cKO mice. Furthermore, OBs from MVNP mice with/without PDL exhibited strong EphB4 staining compared with OBs from the other genotypes. Plump, cuboidal OBs were also more common in MVNP mice than in mice of the other genotypes, including WT mice. Of note, EphB2 and EphB4 staining of OCLs/OBs in MVNP mice with or without PDLs was similar.

Characterization of the role of OCL-Igf1 on OCL differentiation and function. To examine the effects of IGF1 in cells of the OCL lineage on the function of OCL precursors, we cultured CD11b⁺ BM mononuclear cells from 12-month-old mice of each genotype as described in Methods. The number of OCLs formed from OCL precursors obtained from MVNP/*Igf1*-cKO mice treated with RANKL was significantly decreased compared with OCL precursors from MVNP mice (Figure 5A). Similarly, OCL formation from OCL precursors derived from *Igf1*-cKO mice was significantly decreased in response to RANKL treatment compared with OCL precursors from WT mice (Figure 5A). Furthermore, the OCLs formed from MVNP/*Igf1*-cKO mice bone marrow cultures were smaller and had < 20 nuclei/OCL, compared with > 50 nuclei/OCL formed in MVNP mouse bone marrow cultures (Figure 5, B and C).

To further assess the role of OCL-IGF1 in OCL function, we determined the expression levels of cathepsin K and NFATc-1 in purified OCLs formed in vitro. OCLs formed in bone marrow cultures of MVNP/*Igf1*-cKO and *Igf1*-cKO mice expressed lower levels of cathepsin K and NFATc-1 than OCLs formed in cultures from MVNP and WT mice. Cathepsin K levels in OCLs from MVNP/*Igf1*-cKO were decreased by 50% compared with OCLs derived from MVNP mice (Figure 5D). We then tested the bone resorption capacity of these OCLs by plating the same number of mature OCLs on bone slices in the presence of RANKL (50 ng/mL) for 72 hours. OCLs formed in MVNP mouse bone marrow cultures formed numerous large resorption pits. However, OCLs from mice lacking OCL-*Igf1* or WT mice formed low numbers of small pits (Figure 5E). The bone resorption capacity of MVNP/*Igf1*-cKO or *Igf1*-cKO OCLs was significantly decreased compared with OCLs formed in MVNP or WT mouse bone marrow cultures (Figure 5F). In addition, treatment of purified OCL precursors from *Igf1*-cKO or MVNP/*Igf1*-cKO mice with 10 ng/mL of mouse recombinant IGF-1 restored OCL number and nuclear number/OCL to levels present in WT or MVNP-OCLs (Supplemental Fig-

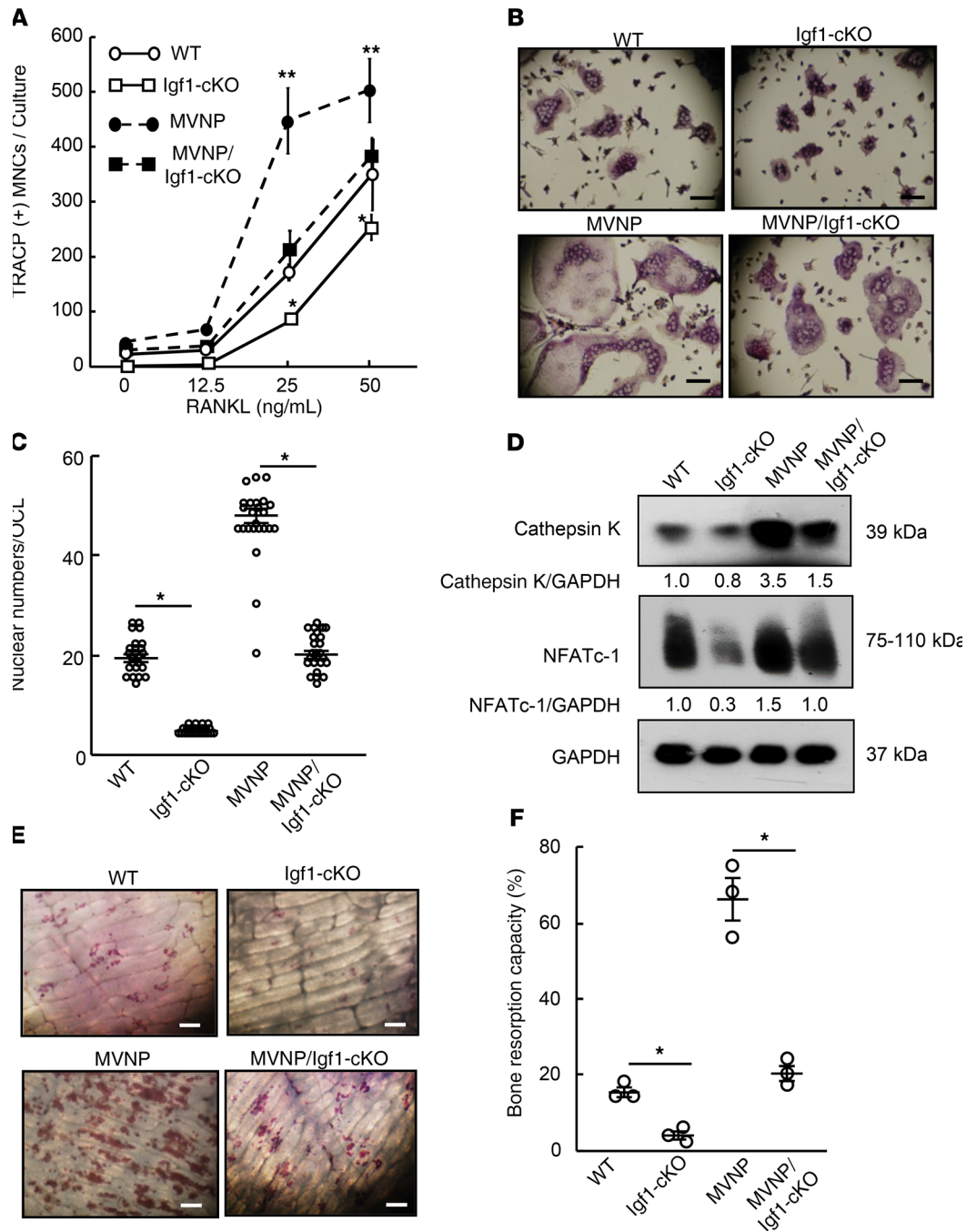


Figure 5. Characterization of OCLs formed in marrow cultures of WT, *Igf1-cKO*, *MVNP*, and *MVNP/Igf1-cKO* mice.

All experiments used BM mononuclear cells from 12-month-old mice. (A) OCLs formation in 4 genotype mice. Results are expressed as the mean \pm SEM from 4 technical replicates from 4 genotype mice. The data were analyzed using a 1-way ANOVA with Tukey test. $*P < 0.05$, $**P < 0.01$ with OCLs from 4 genotype mice. The results are representative of 4 biological replicates. (B) OCL morphology, photomicrographs of OCLs in marrow cultures treated with RANKL (50 ng/mL) and stained with TRACP. Scale bar: 50 μ m. (C) Nuclear numbers per OCL. Results are expressed as the mean \pm SEM of 25 randomly counted OCLs from 4 genotype mice. The data were analyzed using 1-way ANOVA with Tukey test, $*P < 0.01$ as compared with each indicated group. (D) Expression of cathepsin K and NFATc-1. The expression of cathepsin K and NFATc-1 were examined by Western blotting as described in Methods. GAPDH was used as the loading control. Protein expression levels were quantitated by ImageJ software (NIH). The basal ratio for each protein/loading control for OCLs from WT mice was set at 1.0. Results are representative of 3 biological replicates of 4 genotype mice. (E) Photomicrographs of bone resorption area. Bone slices were stained with hematoxylin. Scale bar: 50 μ m. (F) Bone resorption capacity was assayed as described in Methods. Results are expressed as the mean \pm SEM (representative of 3 biological replicated for 4 genotype mice). The data were analyzed using a 1-way ANOVA with Tukey test. $*P < 0.01$ as compared with each indicated group. The results are representative of 4 biological replicates.

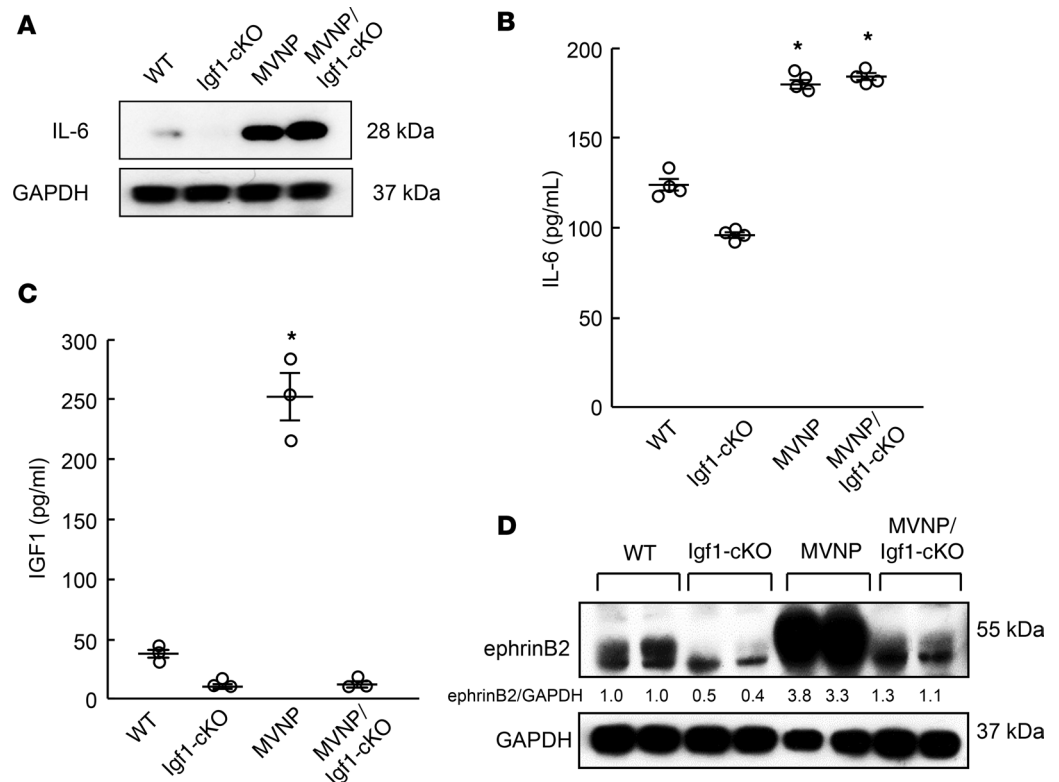


Figure 6. Effects of loss of OCL-*Igf1* on IL-6 and EphB2 expression in OCLs from WT, *Igf1*-cKO, *MVNP*, and *MVNP/Igf1*-cKO mice BM cultures. All experiments used BM mononuclear cells from 12-month-old mice. **(A)** IL-6 expression in OCLs formed in mouse BM cultures. IL-6 expression was assayed by Western blotting using anti-IL-6 antibody as describe in Methods. GAPDH was used as the loading control. Results are representative of 3 different experiments using 3 biological replicates for 4 genotype mice. **(B)** IL-6 levels in culture media. Purified OCLs (5×10^4 cells/mL) from BM cultures derived from the 4 genotypes were cultured with 50 ng/mL of RANKL in α MEM-10% FCS for 72 hours, and CM were used fro ELISA assays of IL-6 and IGF1. The data are shown as mean \pm SEM (4 technical replicates from the 4 genotypes). The data were analyzed using a 1-way ANOVA with Tukey test. * $P < 0.01$ as compared with WT mice. This assay was performed on 2 biological replicates and were similarly. **(C)** IGF1 levels in conditioned media. IGF1 was measured by ELISA as described in Methods. The data are shown as mean \pm SEM (3 biological replicates the from the 4 genotypes). The data were analyzed using 1-way ANOVA with Tukey test. * $P < 0.01$ as compared with WT mice. This assay was performed in 2 individual experiments. **(D)** EphB2 expression in OCLs formed in mouse BM cultures. EphB2 expression was assayed by Western blotting using an EphB2 antibody as described in Methods. The expression levels of EphB2 were quantitated by ImageJ software (NIH). The basal ratio for every protein/loading control from OCLs of WT mice was set at 1.0. Results shown are from 2 biological replicates from the 4 genotypes.

ure 6). Furthermore, *Igf1*-cKO and *MVNP/Igf1*-cKO mice had decreased OCL formation, and these OCLs that formed showed decreased PI3 and Erk kinase activation (Supplemental Figure 7).

IL-6 expression in OCLs is not regulated by IGF1 expression in OCLs. Since IL-6 is a major driver of the abnormal OCL formation in PD (9), we determined if loss of IGF1 in OCLs affected IL-6 expression in OCLs. Therefore, we measured IL-6 production and secretion by highly purified OCLs formed in bone marrow cultures of WT, *Igf1*-cKO, *MVNP*, and *MVNP/Igf1*-cKO mice. OCLs from *MVNP* and *MVNP/Igf1*-cKO mice expressed higher IL-6 levels compared with WT and *Igf1*-cKO mice in the 72-hour cultures (Figure 6A). Importantly, IL-6 levels were similarly significantly increased in conditioned media from both *MVNP* and *MVNP/Igf1*-cKO OCL cultures (Figure 6B). IGF1 levels in *MVNP*-OCL conditioned medium (CM) were 250 ± 23 pg/mL, while IGF1 levels in CM from WT, *Igf1*-cKO, and *MVNP/Igf1*-cKO OCLs were < 50 pg/mL ($P < 0.01$) (Figure 6C). Since deletion of *Igf1* in OCLs did not affect IL-6 expression in OCLs, these results show that increased OCL-IL-6 levels in *MVNP* mice are not dependent on enhanced IGF1 expression in OCLs.

As previously shown (13), EphB2 expression on purified OCLs from *MVNP* mice was increased compared with the other genotypes and was much lower in *MVNP/Igf1*-cKO and *Igf1*-cKO compared with *MVNP* and WT mice, respectively (Figure 6D). IGF1-receptor expression on OCLs was similar in all genotypes (data not shown).

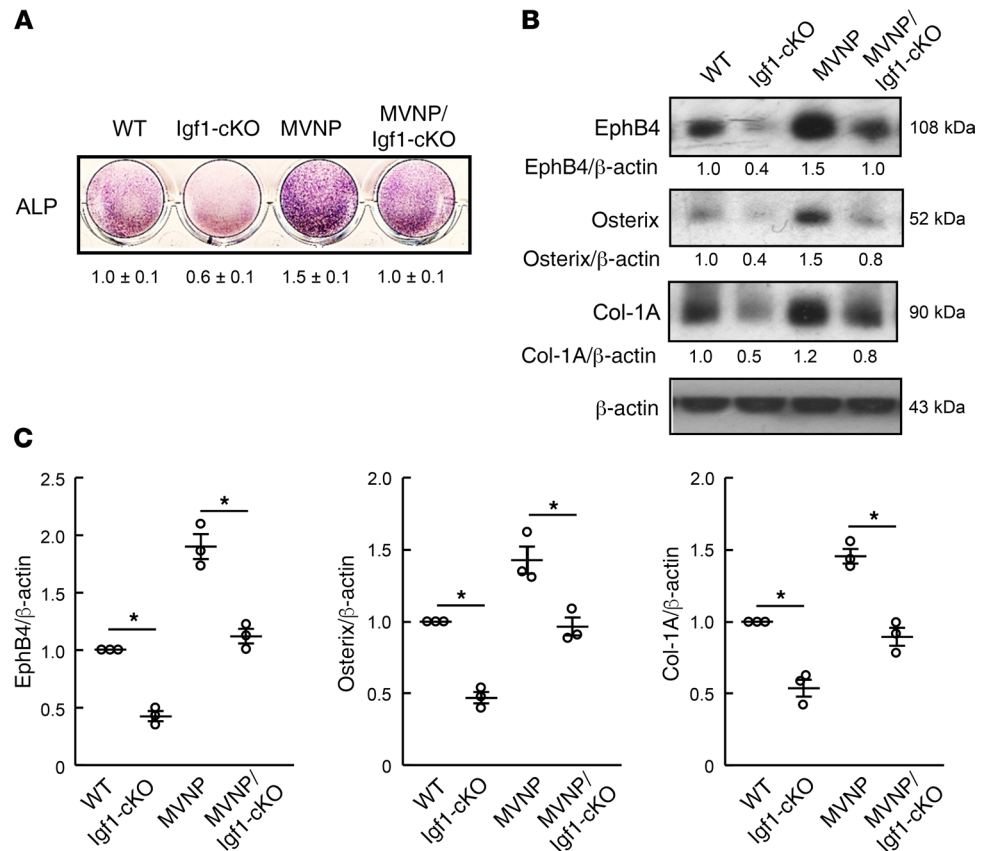


Figure 7. Characteristics of OBs derived from long bones in WT, *Igf1-cKO*, *MVNP*, and *MVNP/Igf1-cKO* mice. All experiments used 12-month-old mice. **(A)** Image of ALP staining of OB outgrowing cells from bone cultured for 14 days. Cells were stained ALP and staining was quantitated by ImageJ software (NIH). Results are representative of 3 biological replicates. **(B)** Expression of OB differentiation maker proteins. The expression of EphB4, osterix, and Col-1A were assessed by Western blotting using anti-EphB4 antibody, anti-osterix antibody, and anti-Col-1A antibody as described in Methods. β-Actin was used as the loading control. The expression levels of EphB4, osterix, and Col-1A were quantitated by ImageJ software (NIH). The basal ratio for every protein/loading control for OBs from WT mice was set at 1.0. Results are representative of 3 biological replicates. **(C)** OB differentiation in cocultures with *MVNP*-OCLs. OCLs (5×10^4 /well) derived from *MVNP* mice were scraped with a rubber policeman as described in Methods and were then replated and cultured with 50 ng/mL RANKL overnight. The OBs (1×10^5 /well) described above were plated on top of the OCLs the next day, and the cells were cocultured for 72 hours. The expression levels of EphB4, osterix, and Col-1A was determined by Western blotting using these antibodies as above. β-Actin was used as the loading control. The expression levels of EphB4, osterix, and Col-1A were quantitated by ImageJ software. The basal ratio of every protein/loading control for OBs from WT mice was set at 1.0. Results are expressed as the mean ± SEM (representative of 3 biological replicated for 4 genotype mice). The data were analyzed using 1-way ANOVA with Tukey test. * $P < 0.01$ as compared with each indicated group. These results of experiment were similarly in 2 different biological replicates.

Characteristics of OBs derived from long bones and their OB differentiation capacity in cocultures with OCLs from MVNP mice. We next determined the differentiation potential of OB precursors derived from bones of WT, *Igf1-cKO*, *MVNP*, and *MVNP/Igf1-cKO* mice (Figure 7A). OBs from *MVNP* mice displayed higher alkaline phosphatase (ALP) activity compared with OBs from the other genotypes. We then determined expression of OB differentiation markers in cell lysates from outgrowth cells of bones from 12-month-old mice cultured for 14 days. Levels of EphB4, osterix, and Col-1A in OBs from *MVNP/Igf1-cKO* and *Igf1-cKO* mice were decreased compared with *MVNP* and WT OBs, respectively (Figure 7B). However, IGF1 receptor levels on OBs derived from these genotypes or WT mice were not significantly different (data not shown).

We found that *MVNP*-OCLs produced high levels of IL-6 and IGF1 (Figure 6, B and C) and induced EphB2 expression in OCLs and EphB4 in OBs in *MVNP* mice in vivo to enhance OB differentiation (Figure 6A and Figure 7B) (13). However, we do not know if loss of OCL-IGF1 in vivo affected the capacity of OBs derived from these mice to differentiate, since these OBs express lower levels of EphB4.

Therefore, we tested the effects of coculturing WT OBs with WT, *MVNP*, or *MVNP/Igf1-cKO* OCLs.

MVNP-OCLs enhanced OB differentiation and increased EphB4 expression on WT OBs compared with coculture with *MVNP/Igfl*-cKO and WT-OCLs. These results support our model that increased OCL-IGF1 produced by *MVNP*-OCLs induces upregulation of EphB4, osterix, and Col-1A to increase OB differentiation (Supplemental Figure 8). We then cocultured OCLs from *MVNP* mice with OBs derived from bones of the 4 genotypes for 72 hours. EphB4, osterix, and Col-1A expression in OBs was measured by Western blot. As shown in Figure 7, EphB4, osterix, and Col-1A expression levels in OBs from *MVNP/Igfl*-cKO and *Igfl*-cKO mice were lower than those of *MVNP* and WT OBs, respectively ($P < 0.05$). EphB4, osterix, and Col-1A levels in OBs were only upregulated in OBs of *MVNP* but not OBs from *MVNP/Igfl*-cKO mice (Figure 7C). These results suggest that the low EphB4 expression by OB precursors from the other genotypes impaired their capacity to respond, in the 72-hour cocultures, to the increased IL-6, IGF1, and EphB2 levels expressed by *MVNP*-OCLs.

Discussion

We previously reported that *MVNP* expression in OCLs from *MVNP* mice and patients with PD induce high levels of IL-6, which upregulate expression of IGF1 and EphB2 in OCLs and EphB4 on OBs (13). These studies provided insights into OCL regulation of OB activity in PD and the potential mechanisms responsible for the enhanced bone formation induced by PD-OCLs. Our in vitro findings suggested that enhanced IL-6 expression and increased IGF1 production by pagetic OCLs may induce the rapid bone formation that occurs in PD. However, the roles of these factors in WT and *MVNP* mice in vivo were unclear. In the current study, we examined the mechanisms responsible and effects of OCL-IGF1 on the increased bone formation and development of bone lesions in PD, as well as in physiologic bone remodeling in vivo.

The liver is the major source of IGF1, and approximately 80% of circulating IGF1 is bound to IGF-binding protein 3 (IGFBP3). OBs and OCys also produce IGF1, which acts as a paracrine and autocrine factor to enhance bone formation. Studies of tissue-specific genetic KO or overexpression of *Igfl* have provided further insights into the importance of local sources of IGF1 in bone. For example, studies of deletion of *Igfl* (19) and overexpression of *Igfl* (20, 21) in OBs or deletion of *Igfl* in OCys (22) showed that IGF1 markedly affects bone formation. These results suggest that changes in local levels of IGF1 in bone are important and not compensated by the high circulating levels of hepatic-derived IGF1. We found that IGF1 was also expressed by OCLs (13). However, the effects of conditional deletion of *Igfl* in OCLs in vivo have not been reported, although the effects of global *Igfl* (23) or *Igfl* receptor (24) KO in mice on OCL activity were reported. Therefore, to determine the contribution of increased OCL-IGF1 that occurs in *MVNP* mice to bone formation in PD, we generated WT and *MVNP* mice with conditional deletion of *Igfl* in OCLs. We confirmed that our *Tracp-Cre* transgene targeted *Cre* to cells in the OCL lineage in bone by generating *Tracp-Cre/ Tomato* mice. We found that *Tracp-Cre(+)/ Tomato* mice showed colocalization of TRACP and Tomato staining in OCLs and, at much lower levels, in scattered OCys in bone (Supplemental Figure 1). Immunostaining OCys with an anti-IGF1 antibody showed similar levels of IGF-expressing OCys in bone sections from the 4 genotypes. Furthermore, we did not find differences either by Western blotting or ELISA assays in IGF1 expression by bone-derived OCys from WT, *Igfl*-cKO, *MVNP*, or *MVNP/Igfl*-cKO mice (Supplemental Figure 2). These results suggest that changes in IGF1 expression by OCys are not responsible for our findings. Since TRACP expression is also detected in the kidney, we measured 1,25-(OH)₂D₃, a calcitropic hormone produced by the kidney. Serum levels of 1,25-(OH)₂D₃ in all 4 genotypes mice were similar. Thus, although TRACP is expressed in kidney, bowel, and other tissues (25), these mice provide a useful model for determining the effects of deletion of *Igfl* in OCLs in bone.

Igfl-cKO and *MVNP/Igfl*-cKO mice were born at much-lower-than-expected numbers. We do not have any data to explain this finding. Possibly, since TRACP is expressed in the placenta and syncytiotrophoblasts (26), the lower numbers of cKO mice may result from insufficient IGF1 expression in the placenta, which affected fetal development.

We found that cKO of *Igfl* in OCLs of *MVNP* or WT mice did not affect femur length, body weight, cortical BV, and serum levels of IGF1 and IGFBP3 (at 20 months of age). These results are in contrast to results of mice with targeted deletion of *Igfl* in the liver. Mice with hepatic *Igfl*-cKO had a 75% decrease in serum IGF1 concentration, with a 26% decrease in cortical BV, mainly affecting the periosteum (27, 28). These results suggest that serum concentrations of IGF1 contribute to earlier acquisition of peak bone mass but do not result in an overall change in bone mass. Since we did not find changes in serum levels of IGF1, or effects on mouse size, body weight, or femoral length, our results suggest that our models reflect the local effects of loss of OCL-IGF1 on bone remodeling — effects that are not compensated for by systemic IGF1 in serum.

In this study, we also examined IGF1 expression in OCLs and BFR in bone specimens from a PD patient and a healthy donor. We confirmed that the abnormal OCLs in the PD patient expressed increased levels of IGF1 and had an increased BFR compared with the healthy donor (Figure 1). These findings supported examining the contribution of increased IGF1 expressed by PD-OCLs to the rapid bone formation in PD and supported determining if IGF1 from normal OCLs also contributes to physiologic bone remodeling.

We found that loss of IGF1 in *MVNP*-OCLs has major effects on the pagetic phenotype of *MVNP* mice. We detected PDLs in 40% of *MVNP* mice, but PDLs were not detected in *MVNP/Igfl-cKO* mice. Furthermore, BV/TV was decreased by 60% in *MVNP/Igfl-cKO* mice compared with *MVNP* mice with PDLs (Figure 2B), and bone mass and OCL and OB surface and numbers in *MVNP/Igfl-cKO* mice were similar to levels in WT mice. Thus, conditional deletion of *Igfl* in OCLs from *MVNP* mice abrogated the pagetic phenotype in *MVNP* mice (Figure 2). Interestingly, our data suggest that OCL-IGF1 mainly affects trabecular bone formation by increasing OCL and OB numbers and surfaces. Furthermore, conditional deletion of OCL-*Igfl* in *MVNP* mice decreased BFR by 80% compared with *MVNP* mice (Figure 3D). These results support that OCL-IGF1 is a major contributor to the pathologic rapid new bone formation that occurs in PD.

Next, we determined if OCL-IGF1 is responsible for the increase in EphB2 and EphB4 in OCLs/OBs of *MVNP* mice. OCLs from *MVNP* mice with/without PDLs displayed much higher IGF1 expression levels compared with OCLs from WT mice. IGF1 was not detected in OCLs from *Igfl-cKO* and *MVNP/Igfl-cKO* mice (Figure 4). EphB2 and EphB4 were increased in OCLs and OBs, respectively, in *MVNP* mice but not in *MVNP/Igfl-cKO* and *Igfl-cKO* mice. These results show that increased OCL-IGF1 expression in *MVNP* mice increased EphB2 expression on OCLs and enhanced EphB4 expression on OBs. Similar to PDLs in patients with PD, PDLs in *MVNP* mice showed increases in OB and OCL parameters (Oc.S/BS, N.Oc/B.Pm, Ob.S/Bs and N.O/B.Pm), mineralized perimeters, MAR, BFR/BS, and larger, more hyper-multinucleated OCLs in bone (Figure 3) compared with *MVNP* mice without PDLs. These results suggest that PDLs may only form in areas of bone with increased numbers of highly active abnormal OCLs and that the high bone turnover state induced by expression of OCL-IGF1 and EphB2 in PD-OCLs contributes to formation of PDLs. The basis for the localized increase in OCL and OB numbers that result in PDLs in PD is currently unknown. Consistent with our results, Wang et al. found that mice lacking the IGF1R in OCLs have decreased EphB2 levels (23). However, their experiments did not determine if IGF1 is expressed by OCLs or if OCL-IGF1 induces EphB2 on OCLs.

Surprisingly we found that cKO of *Igfl* in OCLs does not affect cortical thickness and volume, since these parameters were similar in mice of the 4 genotypes tested (Figure 2, C and D). These results are consistent with those of Zhang et al., who reported that OB-specific *Igflr* KO in mice resulted in a striking decrease in cancellous bone parameters but did not change cortical bone parameters (24).

IGF1 has been shown to be essential for OCL differentiation and to maintain OCL function (29, 30). We found that OCL formation, nuclear number/OCL, and bone resorption capacity of OCLs from *MVNP/Igfl-cKO* and *Igfl-cKO* mice were significantly decreased compared with *MVNP* and WT mice (Figure 5). These results suggest the OCL-derived IGF1 may have autocrine effects on OCL formation in PD and normal bone.

We next examined the mechanism responsible for the increased IGF1 expression in *MVNP*-OCL. We previously found that loss of IL-6 resulted in loss of the pagetic phenotype in *MVNP* mice (9). OCLs formed in bone marrow cultures of *MVNP/IL-6-KO* mice did not display the characteristics of pagetic OCLs. Furthermore, histomorphometric analysis of bones from *MVNP/IL-6-KO* mice showed that loss of IL-6 also abrogated the increase in MAR found in *MVNP* mice and reduced mineralizing perimeter and BFR. However, we did not know if IGF1 increased IL-6 expression. We show here that OCLs from *MVNP/Igfl-cKO* and *MVNP* mice produced similar levels of IL-6 (Figure 6B). Taken together, these results — with our previous findings that showed OCLs from *MVNP/IL6^{-/-}* mice express much lower levels of IGF1 than OCLs from *MVNP* mice (13) — support that IL-6 is an inducer of the pagetic OCL phenotype and contributes to PD. They also suggest that increased IL-6 induced by *MVNP* gene expression in OCLs drives the increased IGF1 expression in OCLs, which in turn is required to increase EphB2 expression in OCLs in *MVNP* mice in vivo. Thus, IL-6 appears to regulate the increased OCL-IGF1 in OCLs from *MVNP* mice in vivo, which plays an important role in the abnormal bone remodeling in PD.

We then determined if OCLs from *MVNP* mice could stimulate the differentiation of OBs from WT, *Igfl-cKO*, *MVNP*, and *MVNP/Igfl-cKO* mice. When OCLs from *MVNP* mice were cocultured with OBs from mice of the 4 genotypes, EphB4, osterix, and Col-1A levels were upregulated to a greater extent in

cocultures containing OBs from *MVNP* mice compared with OBs from WT mice. This increase was lost in cultures containing OBs from *MVNP/Igfl-cKO* mice (Figure 7C). These results further suggest that OCL-IGF1, in addition to IL-6 from PD-OCLs, is necessary to increase bone formation in PD by enhancing bidirectional signaling through increased EphB2/EphB4 *in vivo*.

Finally, we suggest that OCL-IGF1 may play a role in physiologic bone formation. Histological analysis of bones from *Igfl-cKO* mice showed they had lower trabecular BV associated with reduced numbers and size of OCLs compared with WT mice (Figure 2). *In vitro* experiments indicated that loss of OCL-IGF1 was responsible for the decreased OCL generation and bone formation (Figure 5 and Figure 7). These results suggest that OCL-IGF1 may contribute to the maintenance of bone mass in normal adult bone by stimulating OCL differentiation and function that is coupled to bone formation *in vivo*. However, further studies are needed to confirm a role for OCL-Igfl in normal bone formation because we only analyzed a small number of *Igfl-cKO* mice and used only 1 *Cre* model for our study.

In conclusion, our results suggest that OCL-IGF1 increases bone formation and development of PDLs in PD by enhancing bidirectional signaling between OCLs and OBs through increased EphB2/EphB4 *in vivo*.

Methods

Blinding. To avoid bias, all data were collected in a blinded fashion, where the observer was unaware of the experimental group. Key studies were performed by more than 1 individual to determine if there was consistency in the observations.

PD patient and healthy control. The resin embedded bone sections from a PD patient and healthy donor were provided in house. A transiliac crest bone biopsy was taken from a 58-year-old female patient with PD and from a 30-year-old female patient as a healthy control; both were treated with calcein and tetracycline before sampling. The biopsy sample was embedded without decalcification in methyl methacrylate. The sections were stained for TRACP, and IGF1 was detected by an anti-IGF1 antibody (R & D Systems, MAB2911). Histological evaluation was performed under bright-field, fluorescent light, and polarized light. The detailed histological examinations of bone sections from this PD patient and healthy donor were previously reported (9). MAR and BFR/BS were calculated and expressed as recommended to the ASBMR Nomenclature Committee (31–33).

Animal studies. Animals were housed at VCU in individually ventilated cages in a barrier vivarium, which excludes all known mouse viruses and parasites and most bacteria (including helicobacter). The mice were fed standard mouse chow (irradiated Teklad LM-485 diet) and autoclaved water. Mice of both sexes and multiple ages were euthanized under isoflurane anesthesia, followed by cervical dislocation, for collection of bone tissues, which were shipped overnight to IU in DMEM + 10% FBS + penicillin/streptomycin (Sigma Aldrich) at 20°C.

Generation of mice with cKO of *Igfl* in OCLs. Mice with cKO of *Igfl* in OCLs were generated by breeding *Igfl^{fl/fl}* mice that carry *loxP* sequences flanking exon 4 of the gene (17) (The Jackson Laboratory, 016831) with transgenic mice expressing Cre recombinase under the control of a 2.3-kb murine *TRACP* promoter (34) to generate *TRACP-Cre(+)/Igfl^{fl/fl}* mice. These were further bred to *TRACP-MVNP* mice (35, 36), to generate mice of the following 4 genotypes: (a) WT, (b) *Igfl-cKO*, (c) *MVNP*, and (d) *MVNP/Igfl-cKO*. All mice were on a C57BL/6J background. At each generation, only 1 parent carried the *TRACP-MVNP* transgene and only 1 carried the *TRACP-Cre* transgene, so offspring carrying either were homozygous for the transgene. At 12 months of age, body weight was determined and serum IGF1 and IGFBP3 were measured by IGF1-ELISA kit (Abcam, ab100695) and IGFBP3-ELISA kit (Abcam, ab100692). All experiments were performed in mice of both sexes.

TRACP-Cre/ Tomato mice. *TRACP-Cre* mice were bred to a reporter line that contains a CAG promoter-loxSTOPlox-dtTomato transgene inserted into the *ROSA26* locus (Ai9; The Jackson Laboratory, 007909), to generate double-transgenic *TRACP-Cre/ Tomato* mice in which only TRACP-expressing cells should also express the tdTomato protein. We examined the colocalization of TRACP⁺ and Tomato⁺ OCLs by performing TRACP staining and anti-Tomato immunostaining (anti-Tomato antibody from Thermo Fisher Scientific, NC9590225) on serial sections.

μ CT and histomorphometry. Femurs, tibiae, and vertebrae from WT, *Igfl-cKO*, *MVNP*, and *MVNP/Igfl-cKO* at 20 months of age were fixed in 10% buffered formalin at 4°C. Bone microstructure analyses were performed using a μ CT scanning system (viva CT 40, Scanco Medical) with an isotropic voxel size of 10.5 μ m and the scanner settings of 55 kVp, 25 μ A, and 350 ms integration time. Structural parameters were ana-

lyzed in reconstructed 3-dimensional images using evaluation software (μ CT v1.6, Scanco Medical) according to the recommended guideline (18). The regions of interest were defined using previously described methods (37, 38). The cancellous bone and marrow compartments of the L5 vertebral body were examined between the cranial and caudal growth plates. The cortical bones parameters were analyzed in 100 slices at the tibial midshaft, starting 5.5 mm from the proximal metaphysis. The μ CT data were then exported as a sequence of 8-bit DICOM grayscale images, and simultaneous multiplanar reconstructed (MPR) images were viewed using ImageJ software (NIH).

The lumbar vertebrae were decalcified in 10% EDTA at 4°C and embedded in paraffin. The decalcified sections were stained for TRACP, and OCLs containing active TRACP were stained red as described by Liu et al. (39). OCL perimeter (Oc.S/BS) was defined as the length of bone surface covered with TRACP⁺ multinuclear cells. OB perimeter (Ob. S/BS) was also measured in the same field.

Bone formation parameter analysis. To examine bone formation parameters, animals were injected i.p. with calcein (10 mg/kg) 7 days and 2 days before euthanasia. The fifth lumbar vertebra was embedded without decalcification in methyl methacrylate. The undecalcified sections were left unstained for the evaluation of fluorescent labels. The MS/BS, MAR, and BFR/BS were quantified. All variables were expressed and calculated according to the recommendations of the ASBMR Nomenclature Committee (31–33).

Immunohistochemical analysis. The femurs from 20-month-old mice were fixed in 10% buffered formalin and completely decalcified in 10% EDTA at 4°C and embedded in paraffin. Longitudinal sections (5 μ m) were cut and mounted on glass slides. Deparaffinized sections were treated with 1% horse serum for 1 hour, followed by primary antibodies against IGF1 (Abcam, ab9572), EphB2 (Abcam, ab75868), EphB4 (Abcam, ab64820), and control IgG rabbit (Santa Cruz Biotechnology Inc., sc-2027). The sections were incubated overnight and then stained with anti-rabbit IgG conjugated to peroxidase (Vector Laboratories). Scoring was based on staining intensity (positive or negative) and was performed by a blinded observer.

OCL formation from purified OCL precursors. Nonadherent bone marrow cells were harvested and enriched for CD11b⁺ mononuclear cells using CD11b microbeads (MACS, 120-000-300) and a Miltenyi Biotec MACS magnetic cell-sorting system. OCL formation from CD11b⁺ cells was then performed as described previously (13) in the presence of RANKL (R&D Systems) to generate OCLs. The cells were stained for TRACP, and TRACP⁺ multinucleated cells (≥ 3 nuclei/cell) were scored as OCLs.

Isolation of mature OCLs from BM cultures. BM cells flushed from long bones of WT, *Igfl-cKO*, *MVNP*, and *MVNP/Igfl-cKO* mice were cultured in a 10-cm dish (2.5×10^7 cells/dish) with M-CSF (10 ng/mL) (R&D Systems) for 3 days and RANKL (50 ng/mL) (R&D Systems) for 4 days as previously described (13). At the end of culturing, trypsin-EDTA (Corning) was added, and the cultures were incubated for 3 minutes to remove nonosteoclastic cells and enrich the concentration of OCLs in the cultures.

Bone resorption assays. OCLs generated as described above were cultured on bovine bone slices (Immunodiagnostic Systems, DT-1BON1000-96) in α MEM (Thermo Fisher Scientific) containing 10% FCS (Sigma-Aldrich) and RANKL (50 ng/mL). After 7 days of culture, the cells were removed, the bone slices were stained with acid hematoxylin, and the areas of dentin resorption were determined as previously described (40).

Isolation and culture of primary OBs. After flushing the BM from tibiae and femurs of WT, *Igfl-cKO*, *MVNP*, and *MVNP/Igfl-cKO* mice, the tibiae and femurs were cultured in α MEM containing 10% FCS for 7–10 days. The bones were then placed in 60-mm dishes, and the cultures continued in α MEM containing 10% FCS until cells growing out of the bones formed a confluent monolayer. The original bone was removed, and the outgrowth cells from the bone were treated with 0.25% trypsin and 0.05% EDTA for 10 minutes at 37°C. These cells were used as primary OBs without further passage. The primary OBs (2×10^5 cells/well in 6-well plates) were cultured in α MEM containing 10% FCS for 7–14 days. Cells were either stained for ALP or alizarin red, or cell lysates were collected and analyzed for protein expression, as previously described (13).

Coculture of OCLs and OBs. OCLs (2×10^4 cells/well in 12-well plates) derived from cultures of *MVNP*-OCL precursors were scraped with a rubber policeman as described above, replated, and cultured with 50 ng/mL RANKL overnight. The OBs (1×10^5 cells/well) described above were plated on top of the OCLs the next day, and the cells were cocultured for 72 hours.

Isolation and culture of primary osteocyte-like cells. Primary OBs (1×10^5 cells/mL/well in 12-well plates) isolated as described above were cultured in α MEM containing 10% FCS for 30 days. Cells were analyzed for OCy markers sclerostin, DMP1, and ORP150 (Supplemental Figure 2) by Western blotting and used to determine IGF1 production by OCys isolated from femurs of the 4 genotypes.

Immunoblotting. Total proteins were extracted from OCLs, OBs, or OCys, with RIPA buffer and the cell

lysates (10 µg/lane) loaded on SDS gels using Bio-Rad Mini-PROTEAN Precast Gels. The resolved proteins were transferred onto nitrocellulose membranes (TGX Membrane; Bio-Rad) using the Trans-Blot Turbo Transfer System (Bio-Rad); then, the membranes were stained with Ponceau S and cut into strips based on the molecular weight markers. Membranes were then exposed to primary antibodies overnight at 4°C and incubated with IgG HRP-conjugated antibody for 1 hour. The blots were washed and visualized by a Super Signal West Dura Extended Duration System (Cell Signaling). Antibodies used for detection of EphB2 (Abcam, ab75868), EphB4 (Abcam, ab64820), IGF1 (Abcam, ab63926), IGF1R (Abcam, ab39398), osterix (Abcam, ab22552), β-actin (Abcam, ab49900), NFATc-1 (Santa Cruz Biotechnology Inc., sc-7294), cathepsin K (Santa Cruz Biotechnology Inc., sc-48353), IL-6 (Santa Cruz Biotechnology Inc., sc-7920), Col-1A (MilliporeSigma, AB765P), DMP1 (Novus Biological, NRP1-45525), Sclerostin (Abcam, ab63097), ORP150 (Santa Cruz Biotechnology Inc., sc-398224), and GAPDH (Cell-Signaling Technology, 3683)

IGF1 and IL-6 ELISA assays. Mouse OCLs were isolated as described above, and OCLs (5×10^4 cells/mL) were cultured with RANKL for 3 days. OCys (2×10^5 cells/mL) were cultured in α MEM 10%FCS for 3 days. Conditioned media from these cultures were harvested at the end of the culture period, and the concentration of IGF1 was measured using an ELISA kit for murine IGF1 (Abcam, ab100695). IL-6 was measured in OCL-CM using an ELISA kit for murine IL-6 (R&D system, M600B) according to the manufacturer's instructions.

Measurement of serum 1,25-(OH)₂D₃. Mouse serum 1,25-dihydroxyvitamin D₃ levels were measured with an ELISA Kit (CUSABIO, CSB-E13697m) according to the manufacturer's instructions.

Statistics. Significance was evaluated using a 1-way ANOVA with a Tukey test. Differences with $P < 0.05$ were considered significant.

Study approvals. All animal studies were performed as described in approved IACUC protocols from VCU and IU and ACURO protocol from the Department of Defense, in accordance with the principles and procedures outlined in the *Guide for the Care and Use of Laboratory Animals* (National Academies Press, 2011).

Author contributions

JMC, GDR, and NK designed the study, interpreted the data, and wrote the manuscript. KM, YO, JT, JDC, and NK performed the experiments. JJW and MAS generated the transgenic mice, and JJW helped write the manuscript. KM, HZ, and DDD performed histological studies and analyses. All authors approved the submission of the manuscript.

Acknowledgments

This work was supported by grants from the National Institute of Arthritis and Musculoskeletal and Skin Diseases (NIAMS), NIH (R01-AR057308, to GDR); the National Cancer Institute (NCI), NIH (5P30CA016059, to JJW); and the US Department of Defense (W81XWH-12-1-0533, to NK). The mice for this research were provided by the VCU Transgenic/Knock-out Mouse Shared Resource. We thank Mohammad S. Khalid for his technical assistance of immunostaining.

Address correspondence to: G. David Roodman, Department of Medicine, Hematology/Oncology, School of Medicine, Indiana University, 980 West Walnut Street, Suite C312, Indianapolis, Indiana 46204, USA. Phone: 317.278.6255; Email: groodman@iu.edu.

1. Basle M, Minard MF, Rebel A. [Structure and ultrastructure of osteoblasts and of the osteoid tissue in Paget's disease of bone (author's transl)]. *Pathol Biol.* 1978;26(8):475–479.
2. Zajac AJ, Phillips PE. Paget's disease of bone: clinical features and treatment. *Clin Exp Rheumatol.* 1985;3(1):75–88.
3. Rebel A, Malkani K, Baslé M, Bregeon C. Osteoclast ultrastructure in Paget's disease. *Calcif Tissue Res.* 1976;(2):187–199.
4. Roodman GD, Windle JJ. Paget disease of bone. *J Clin Invest.* 2005;115(2):200–208.
5. Kukita A, Chenu C, McManus LM, Mundy GR, Roodman GD. Atypical multinucleated cells form in long-term marrow cultures from patients with Paget's disease. *J Clin Invest.* 1990;85(4):1280–1286.
6. Kurihara N, et al. Role of TAFII-17, a VDR binding protein, in the increased osteoclast formation in Paget's Disease. *J Bone Miner Res.* 2004;19(7):1154–1164.
7. Mena C, et al. Enhanced RANK ligand expression and responsivity of bone marrow cells in Paget's disease of bone. *J Clin Invest.* 2000;105(12):1833–1838.
8. Roodman GD, et al. Interleukin 6. A potential autocrine/paracrine factor in Paget's disease of bone. *J Clin Invest.* 1992;89(1):46–52.
9. Kurihara N, et al. Contributions of the measles virus nucleocapsid gene and the SQSTM1/p62(P392L) mutation to Paget's disease. *Cell Metab.* 2011;13(1):23–34.
10. Matsuo K, Otaki N. Bone cell interactions through Eph/ephrin: bone modeling, remodeling and associated diseases. *Cell Adh*

- Migr.* 2012;6(2):148–156.
11. Zhao C, et al. Bidirectional ephrinB2-EphB4 signaling controls bone homeostasis. *Cell Metab.* 2006;4(2):111–121.
 12. Edwards CM, Mundy GR. Eph receptors and ephrin signaling pathways: a role in bone homeostasis. *Int J Med Sci.* 2008;5(5):263–272.
 13. Teramachi J, et al. Measles virus nucleocapsid protein increases osteoblast differentiation in Paget's disease. *J Clin Invest.* 2016;126(3):1012–1022.
 14. Tahimic CG, Wang Y, Bikle DD. Anabolic effects of IGF-1 signaling on the skeleton. *Front Endocrinol (Lausanne).* 2013;4:6.
 15. Xian L, et al. Matrix IGF-1 maintains bone mass by activation of mTOR in mesenchymal stem cells. *Nat Med.* 2012;18(7):1095–1101.
 16. Wang Y, Nishida S, Elalieh HZ, Long RK, Halloran BP, Bikle DD. Role of IGF-I signaling in regulating osteoclastogenesis. *J Bone Miner Res.* 2006;21(9):1350–1358.
 17. Liu JL, et al. Insulin-like growth factor-I affects perinatal lethality and postnatal development in a gene dosage-dependent manner: manipulation using the Cre/loxP system in transgenic mice. *Mol Endocrinol.* 1998;12(9):1452–1462.
 18. Bouxsein ML, Boyd SK, Christiansen BA, Guldberg RE, Jepsen KJ, Müller R. Guidelines for assessment of bone microstructure in rodents using micro-computed tomography. *J Bone Miner Res.* 2010;25(7):1468–1486.
 19. Govoni KE, Wergedal JE, Florin L, Angel P, Baylink DJ, Mohan S. Conditional deletion of insulin-like growth factor-I in collagen type I α 2-expressing cells results in postnatal lethality and a dramatic reduction in bone accretion. *Endocrinology.* 2007;148(12):5706–5715.
 20. Zhao G, et al. Targeted overexpression of insulin-like growth factor I to osteoblasts of transgenic mice: increased trabecular bone volume without increased osteoblast proliferation. *Endocrinology.* 2000;141(7):2674–2682.
 21. Jiang J, et al. Transgenic mice with osteoblast-targeted insulin-like growth factor-I show increased bone remodeling. *Bone.* 2006;39(3):494–504.
 22. Sheng MH, Zhou XD, Bonewald LF, Baylink DJ, Lau KH. Disruption of the insulin-like growth factor-I gene in osteocytes impairs developmental bone growth in mice. *Bone.* 2013;52(1):133–144.
 23. Wang Y, Menendez A, Fong C, ElAlieh HZ, Chang W, Bikle DD. Ephrin B2/EphB4 mediates the actions of IGF-I signaling in regulating endochondral bone formation. *J Bone Miner Res.* 2014;29(8):1900–1913.
 24. Zhang M, et al. Osteoblast-specific knockout of the insulin-like growth factor (IGF) receptor gene reveals an essential role of IGF signaling in bone matrix mineralization. *J Biol Chem.* 2002;277(46):44005–44012.
 25. Chiu WS, McManus JF, Notini AJ, Cassady AI, Zajac JD, Davey RA. Transgenic mice that express Cre recombinase in osteoclasts. *Genesis.* 2004;39(3):178–185.
 26. Hiden U, Glitzner E, Hartmann M, Desoye G. Insulin and the IGF system in the human placenta of normal and diabetic pregnancies. *J Anat.* 2009;215(1):60–68.
 27. Yakar S, et al. Circulating levels of IGF-1 directly regulate bone growth and density. *J Clin Invest.* 2002;110(6):771–781.
 28. Elis S, et al. Elevated serum levels of IGF-1 are sufficient to establish normal body size and skeletal properties even in the absence of tissue IGF-1. *J Bone Miner Res.* 2010;25(6):1257–1266.
 29. Fiorelli G, et al. Characterization and function of the receptor for IGF-I in human preosteoclastic cells. *Bone.* 1996;18(3):269–276.
 30. Bikle D, et al. The skeletal structure of insulin-like growth factor I-deficient mice. *J Bone Miner Res.* 2001;16(12):2320–2329.
 31. Parfitt AM, et al. Bone histomorphometry: standardization of nomenclature, symbols, and units. Report of the ASBMR Histomorphometry Nomenclature Committee. *J Bone Miner Res.* 1987;2(6):595–610.
 32. American Society for Bone Mineral Research President's Committee on Nomenclature. Proposed standard nomenclature for new tumor necrosis factor family members involved in the regulation of bone resorption. The American Society for Bone and Mineral Research President's Committee on Nomenclature. *J Bone Miner Res.* 2000;15(12):2293–2296.
 33. Dempster DW, et al. Standardized nomenclature, symbols, and units for bone histomorphometry: a 2012 update of the report of the ASBMR Histomorphometry Nomenclature Committee. *J Bone Miner Res.* 2013;28(1):2–17.
 34. Dossa T, et al. Osteoclast-specific inactivation of the integrin-linked kinase (ILK) inhibits bone resorption. *J Cell Biochem.* 2010;110(4):960–967.
 35. Kurihara N, et al. Expression of measles virus nucleocapsid protein in osteoclasts induces Paget's disease-like bone lesions in mice. *J Bone Miner Res.* 2006;21(3):446–455.
 36. Reddy SV, Singer FR, Mallette L, Roodman GD. Detection of measles virus nucleocapsid transcripts in circulating blood cells from patients with Paget disease. *J Bone Miner Res.* 1996;11(11):1602–1607.
 37. Glatt V, Canalis E, Stadmeier L, Bouxsein ML. Age-related changes in trabecular architecture differ in female and male C57BL/6J mice. *J Bone Miner Res.* 2007;22(8):1197–1207.
 38. Colaianni G, et al. Deletion of the Transcription Factor PGC-1 α in Mice Negatively Regulates Bone Mass. *Calcif Tissue Int.* 2018;103(6):638–652.
 39. Liu B, Yu SF, Li TJ. Multinucleated giant cells in various forms of giant cell containing lesions of the jaws express features of osteoclasts. *J Oral Pathol Med.* 2003;32(6):367–375.
 40. Ishizuka S, Kurihara N, Reddy SV, Cornish J, Cundy T, Roodman GD. (23S)-25-Dehydro-1 α -hydroxyvitamin D₃-26,23-lactone, a vitamin D receptor antagonist that inhibits osteoclast formation and bone resorption in bone marrow cultures from patients with Paget's disease. *Endocrinology.* 2005;146(4):2023–2030.